Theor Chem Acc (2011) 130:891–900
DOI 10.1007/s00214-010-0803-x

REGULAR ARTICLE

An unsymmetrical behavior of reactant units in the Kolbe–Schmitt reaction

Shinichi Yamabe · Shoko Yamazaki

Received: 12 March 2010 / Accepted: 21 August 2010 / Published online: 5 September 2010

Abstract Paths of the Kolbe–Schmitt reaction were investigated by the use of RB3LYP/6-311(+)G(d,p) density functional theory calculations. In a monomer model composed of $C_6H_5O^-$, Na^+ and CO_2 affording sodium salicylate [$C_6H_4(OH)CO_2{}^-Na^+$], a proton-shift step (Z Naturforsch 57a:812, 2002) was found to have an unrealistically large activation energy. In consideration of the phenol volatilization in the Kolbe's experiment and the need of the linearity of the proton-transfer path, a dimer model was constructed. Again, a mutual proton-transfer step has a large activation energy. Alternatively, in a dimer model, a transfer path where the phenoxide ion in one monomer acts as a proton acceptor was found to have a reasonable energy. Addition of one more sodium ion leads to the significant lowering of activation energies. Thus, in the dimer, two monomers behave differently (A + A → A + B); one is as if it were a catalyst.

Keywords Kolbe–Schmitt reaction · Density functional theory calculations · Dimer model · Proton transfer · Sodium salicylate

Dedicated to Professor Akira Imamura on the occasion of his 77th birthday and published as part of the Imamura Festschrift Issue.

Electronic supplementary material The online version of this article (doi:10.1007/s00214-010-0803-x) contains supplementary material, which is available to authorized users.

S. Yamabe (✉) · S. Yamazaki
Department of Chemistry, Nara University of Education, Takabatake-cho, Nara 630-8528, Japan
e-mail: yamabes@nara-edu.ac.jp

1 Introduction

The Kolbe–Schmitt reaction is defined in Scheme 1 [1]. In 1860, Hermann Kolbe found that the sodium phenoxide salt reacts with CO_2 at the standard pressure ($P = 1$ atm) and high temperatures (100–250 °C) to afford sodium salicylate [2]. The salicylate was dissolved in water and the salicylic acid (*o*-hydroxybenzoic acid) precipitated on acidification by H_2SO_4.

In 1874, he proposed an improved procedure for the preparation of the salicylic acid, which is shown in Scheme 2 [3]. The PhO^-Na^+ salt was prepared by evaporating an aqueous solution of equimolar amounts of PhOH and NaOH to dryness. The dried salt was heated to 180 °C, and CO_2 was allowed to pass slowly over it. The temperature was raised to 220–250 °C, and the reaction was terminated, when no more phenol distilled. Owing to the volatilization of the phenol, the yield of the salicylic acid could not exceed 50%.

In 1885, Rudolf Schmitt found that the condition of high temperatures (100–130 °C) and high pressures (80–94 atm) gave an excellent yield (94–97%) of the salicylic acid [4]. For example, at $T = 100$ °C, the yield is 94% along with two by-products, *p*-hydroxybenzoic acid (4%) and 4-hydroxyisophthalic acid (2%). The high pressure is thought to suppress the loss of phenol by the volatilization.

In the *ortho–para* orientation of electrophilic aromatic substitutions, usually the *para* product is major and the *ortho* one is minor. The above ratio (*ortho* 94% to *para* 4%) suggests that the cation-coordinated addition–elimination takes place preferentially at the *ortho* position. A mild condition ($T = 25$ °C and $P = 64.5$ atm) for the Kolbe–Schmitt reaction was examined [5]. The yields were 32.30% (*ortho*, main product) and 4.60% (*para*) along with

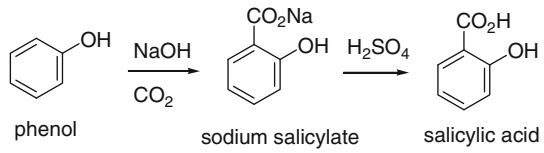

Scheme 1 The Kolbe–Schmitt reaction

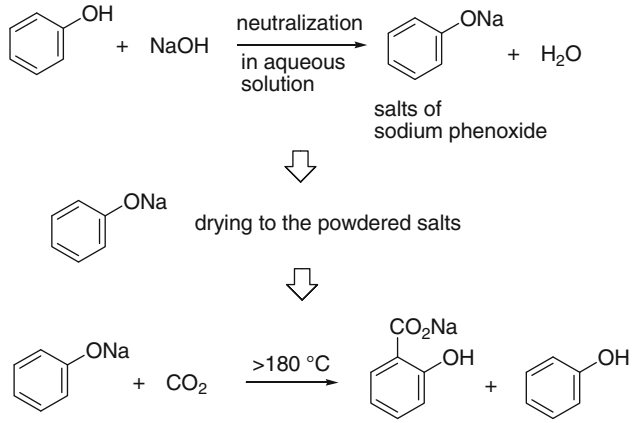

Scheme 2 Kolbe's experiment made in 1874 [3]. The drying procedure is necessary, because strong chelation of water molecules with sodium phenoxide prevents the initial electrophilic addition of CO_2

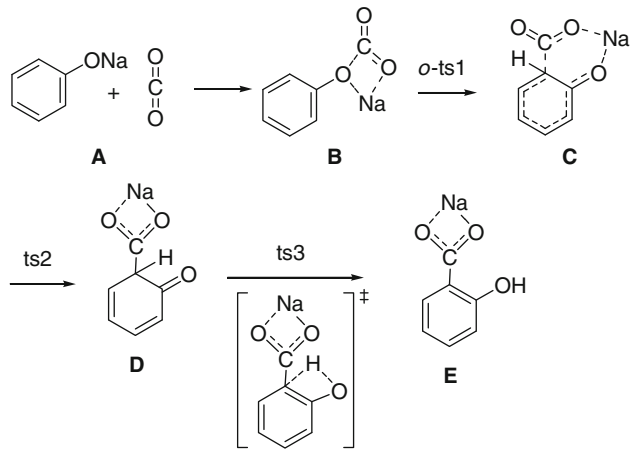

Scheme 3 A reaction path obtained by RB3LYP/LAN2DZ calculations [10]. "*o*-ts1" means the first transition state of the CO_2 *ortho* addition, which follows the Dewar's model [9]

that of phenol. Thus, formation of the *para*-hydroxybenzoic acid occurs simultaneously.

Many studies have been made to determine the reaction mechanism of this classic reaction [4–13]. Two NaOPh-CO_2 intermediates with ν (CO_2, asymm) = 1,685 cm^{-1} and ν (CO_2, asymm) = 1,680, 1,651 cm^{-1} are thought to be involved in it [7]. A mechanism based on the preliminary association of PhO^-Na^+ with CO_2 to form a complex and an intramolecular displacement of the *ortho*

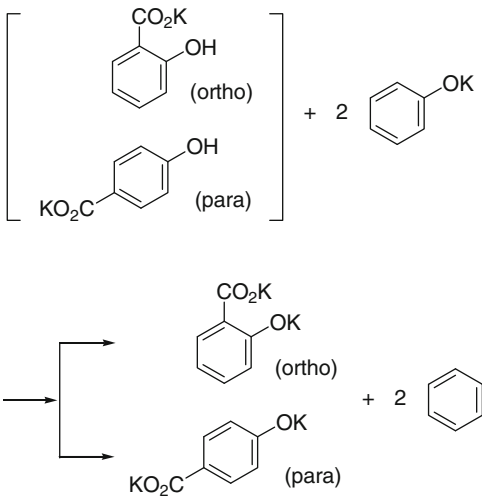

Scheme 4 An explanation for formation of phenol [16]

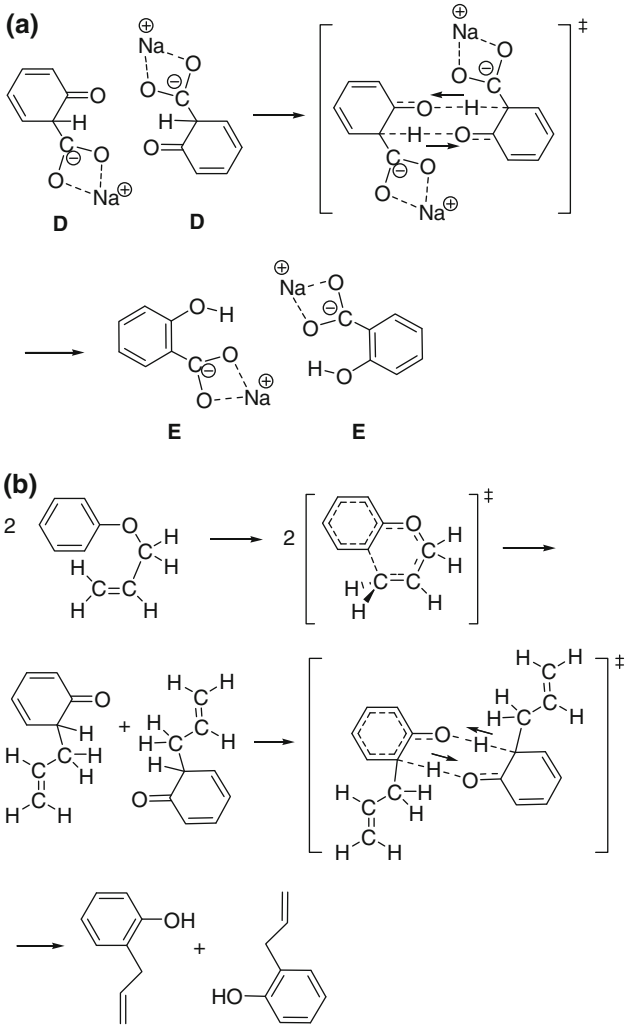

Scheme 5 **a** A mutual proton shift for the isomerization, D → E. Species D and E are defined in Scheme 3. **b** The Claisen shift of allyl phenyl ether to ortho-allyl phenol [17]

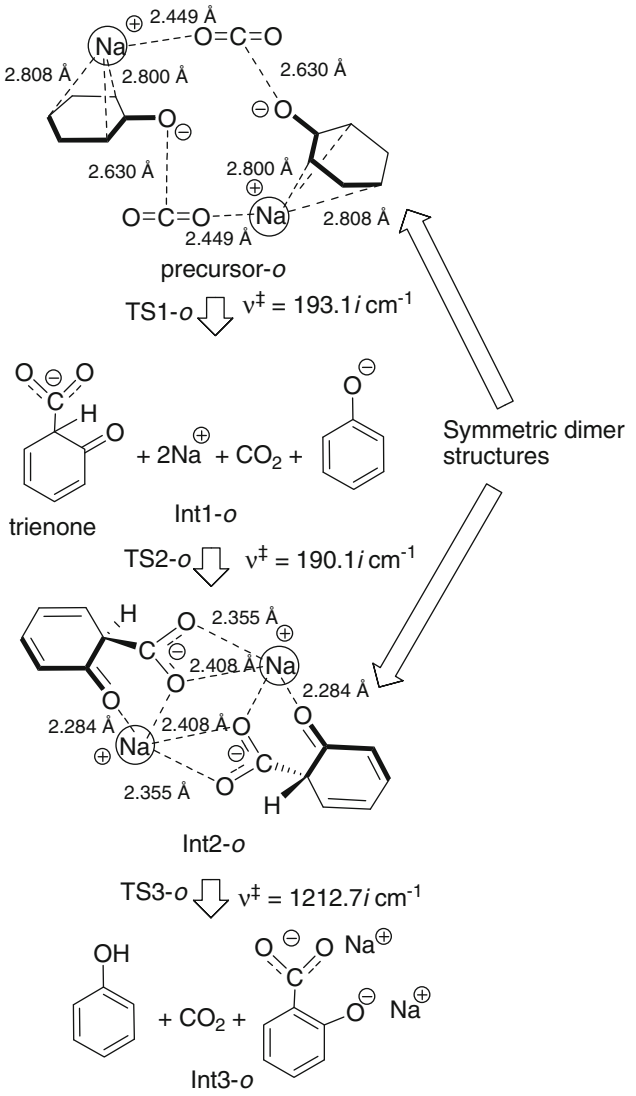

Scheme 6 A calculated path in line with that in Scheme 5a. Symmetry in precursor and Int2-*o* has been broken in Int3-*o*. That is, one CO_2 adduct has been dissociated. Geometries of precursor-*o*, TS1-*o* and Int1-*o* are shown in Fig. 2. Those of TS2-*o*, Int2-*o*, TS3-*o* and Int3-*o* are in Fig. S2 (Supplementary material)

hydrogen by electrophilic attack was suggested [8]. Dewar proposed a reaction model shown in Scheme 3 [9]. A DFT calculation was made, following the model [10].

In the scheme, species A is composed of free PhONa and CO_2 molecules. In species B, they are bound with each other. In the (B → C) step, i.e., *o*-ts1, CO_2 is added to the *ortho* position of the phenoxide ring. In (C → D), ts2, the sodium ion is shifted to only the carboxylate group. In (D → E), ts3, the *ortho* proton is shifted to the oxygen. Although the calculated process is straightforward, the activation energy (+45.67 kcal/mol relative to the energy of species D, +65.69 kcal/mol relative to that of A) of ts3 is too large for the reaction to occur. By nature, the [1, 3] H rearrangement is "symmetry forbidden" according to the

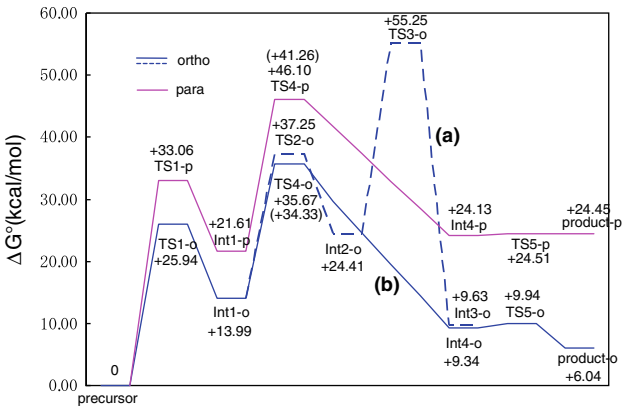

Fig. 1 Changes of RB3LYP/6-311(+)G(d,p) Gibbs free energies ($T = 298.15$ K, $P = 1$ atm) for reactions of the dimer model in Scheme 6. In *parentheses*, RB3PW91 ΔG values are shown

Woodward–Hoffmann (W–H) rules [14, 15] and is improbable. In addition, formation of phenol (which should be involved in the reaction path) cannot be explained by the unimolecular model in Scheme 3. In fact, a bimolecular model, $C_6H_4(OH)COOK + C_6H_5OK \rightarrow C_6H_4(OK)COOK + C_6H_5OH$, was suggested for the formation (Scheme 4) [16].

The isomerization step, ts3 (D → E) in Scheme 3, appears to be critical to consider the mechanism. The species D is a trienone and would be stable. The driving force of the isomerization, i.e., of hydrogen transfer from Cα to ketone O, keto-enol tautomerization of the species D, is thought to be the aromatization of the ring. A candidate of the isomerization is shown in Scheme 5a. Intermolecular and simultaneous proton shifts, (D + D) → (E + E), might give an activation energy smaller than that of ts3. In our previous work, a double-proton transfer of Scheme 5b was found to be of a much smaller energy than that of the intramolecular and direct [1, 3] H-shift in the second step of the Claisen rearrangement [17].

In this work, the mechanism was investigated computationally by the use of a dimer model, $(PhONa + CO_2)_2$. The deprotonation of the trienone (D) and formation of phenol were scrutinized carefully.

2 Method of calculations

The geometries were determined by density functional theory calculations at the RB3LYP/6-311(+)G(d,p) [18–20], where diffuse orbitals "(+)" are added to the oxygen 6-311G(d,p) basis set. For a large system, $(PhONa\text{-}CO_2)_2 + Na^+ + (CO_2)_6$, RB3LYP/6-31G(d) calculations were made (Fig. 7). Key transition state geometries were examined with B3PW91 calculations [20–23]. The obtained data are shown in parentheses in Figs. 2, 3, 4 and 5. B3PW91,

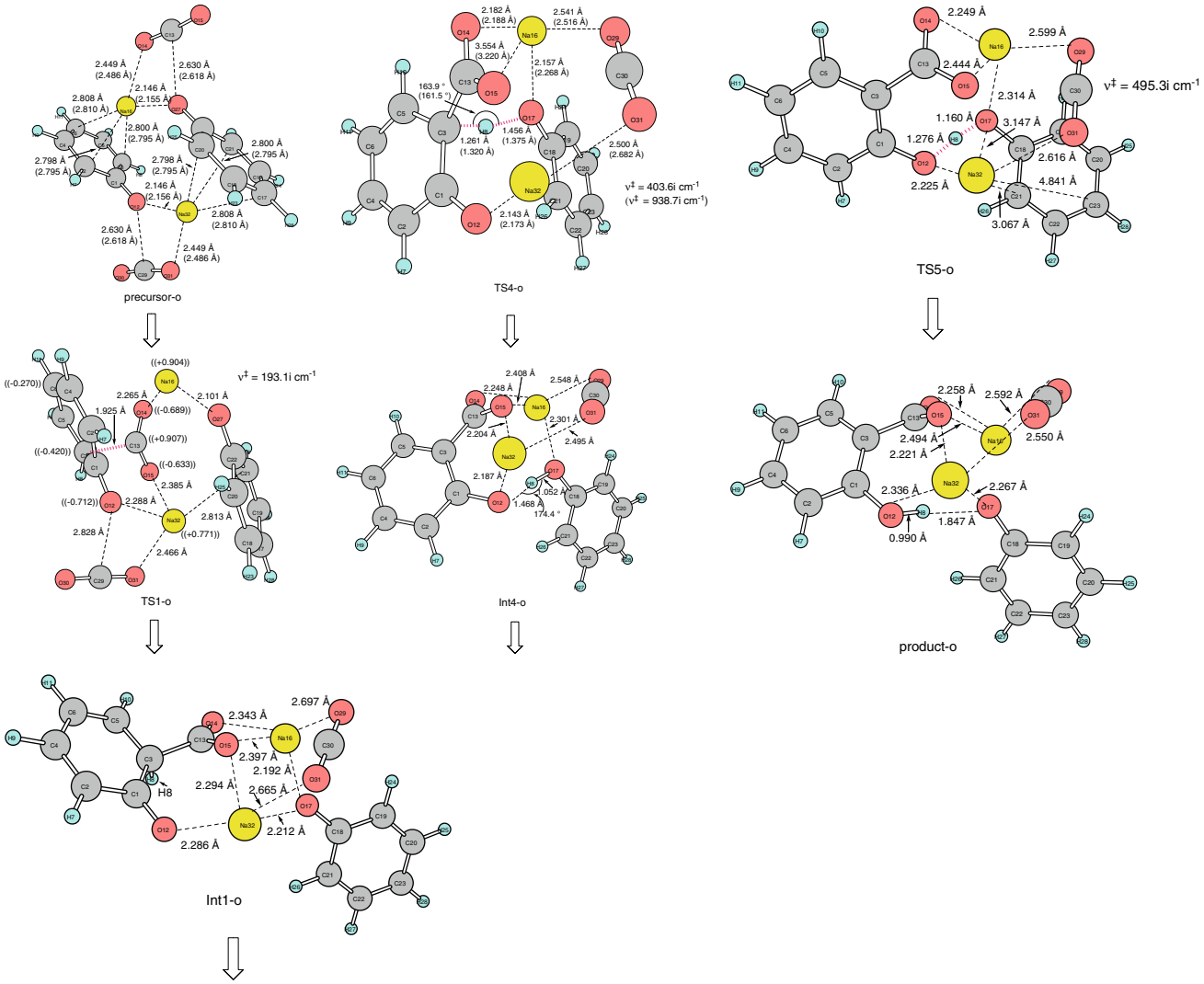

Fig. 2 Alternative unsymmetrical route and the geometries of a dimer model (PhONa + CO_2)$_2$, which leads to the sodium salicylate. Numerical data shown on the precursor and the key transition state geometries without parentheses are of B3LYP/6-311(+)G(d,p) and those in parentheses are of B3PW91/6-311(+)G(d,p). In TS1-o, natural charges of the natural population analysis are shown in *double parentheses*

M05 [24], M06 [25, 26] and PBE1KCIS [27] with the 6-311(+)G(d,p) basis set were carried out on the precursor (B) and the proton shift TS (ts3) in Fig. S1 (Supporting Information). RB3LYP/aug-cc-pVDZ [28, 29] calculations were also made on B and ts3. TSs were characterized by vibrational analysis, by which we examined whether the Hessian matrices obtained from TS geometries had single imaginary frequencies ($\nu^{\ddagger}$). From the TSs, reaction paths were followed using the IRC (intrinsic reaction coordinate) method [30, 31] to obtain the minimum-energy geometries. Relative Gibbs free energies were calculated by thermal correction (T = 298.15 K, P = 1 atm) energies. The natural population analysis of NBO [32] was carried out for **C** in Fig. S1 and TS1-o in Fig. 2. All calculations were carried out using the GAUSSIAN 03 [33] program package installed at Research Center for Computational Science, Okazaki, Japan.

3 Results and discussions

3.1 Dimer model, (PhO^{-}Na^{+}CO$_2$)$_2$

The Dewar's unimolecular model (Scheme 3) was investigated first. The calculated results are shown in Fig. S1 (Supplementary material). The activation free energy of ts3 ($\Delta G^{\ddagger}$ = 65.69 kcal/mol relative to the energy of B) is shown to be significant. Second, a dimer model was investigated. At the top of Scheme 6, a symmetric (point group i) geometry was shown as "precursor-*o*". Each sodium ion is linked weakly with the phenoxide oxygen, π electronic cloud in the η6 coordination and one oxygen atom of CO_2. One CO_2 molecule adds to the *ortho* position electrophilically at TS1-*o*. Here, TS1-*o* means the first transition state for the *ortho* addition. The trienone-

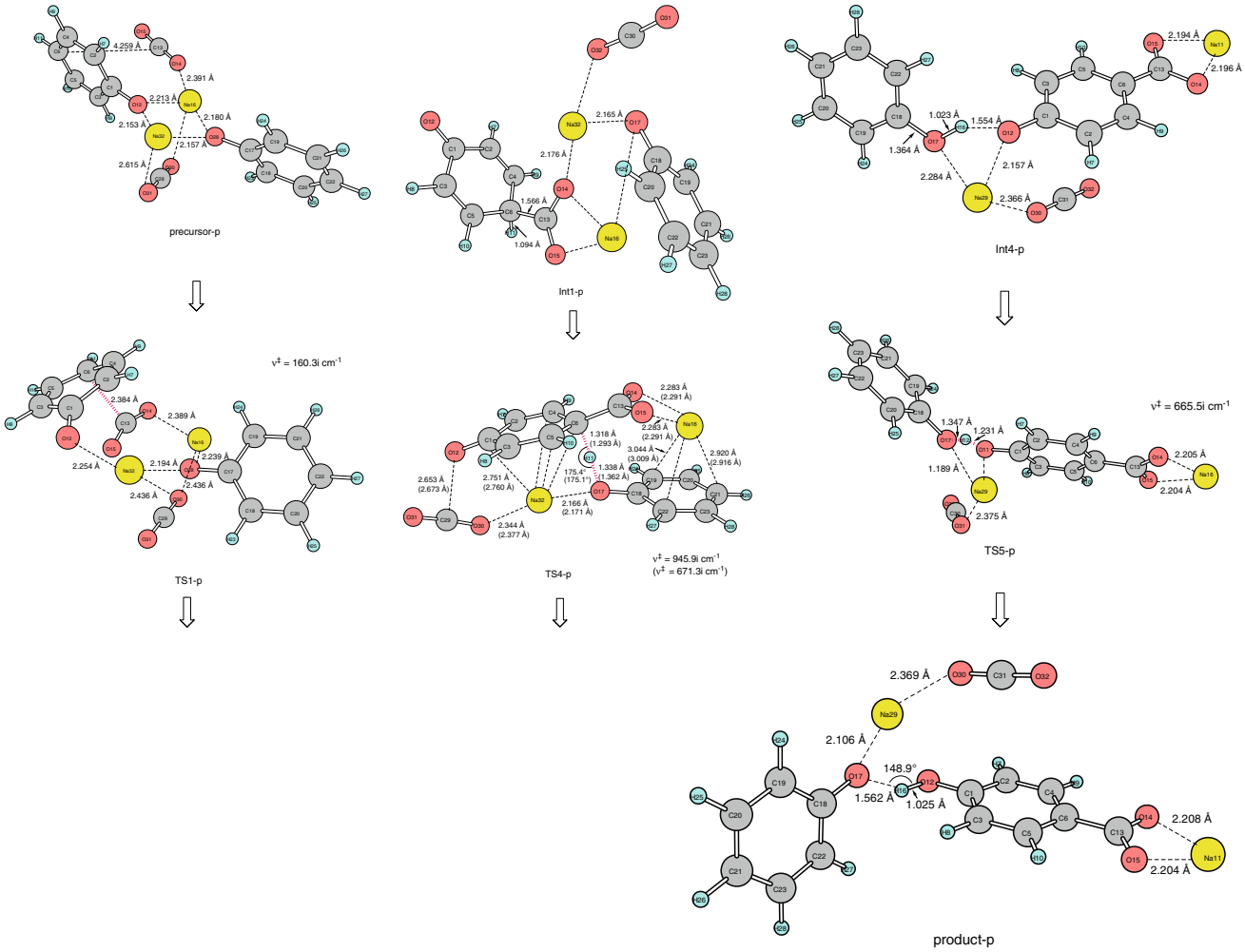

Fig. 3 Geometric changes in the dimer model, which leads to the sodium para-hydroxy benzoate

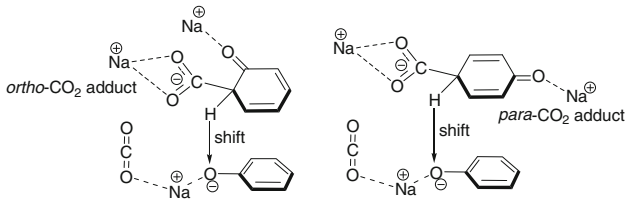

Scheme 7 How is the proton H-shift brought about from the neutral CO_2 adducts ($C_6H_5OCO_2Na$)? One more Na^+ ion is added to the $(PhO^- + CO_2 + Na^+)_2$ system to enhance the proton shift. So far, the solvent effect on the Kolbe–Schmitt reaction was discussed only in DFT calculations of the monomer model of Scheme 3 [34]

containing intermediate, Int1-*o*, results. After Int1-*o*, the second electrophilic CO_2 attack occurs at TS2-*o*. A symmetric structure involving the trienone dimer is reached (Int2-*o*). From Int2-*o*, proton shifts illustrated in Scheme 5a were expected. However, the mutual proton-shift path could not be obtained. Alternatively, a TS geometry with one-proton shift (TS3-*o*) was found. TS3-*o* involves the CO_2 dissociation as well as the proton shift. The resultant intermediate, Int3-*o*, consists of phenol, CO_2 and disodium salicylate ($C_6H_4ONaCO_2Na$). Thus, two ($PhO^-Na^+CO_2$) units were found to behave in a way (Scheme 6) different from that predicted in Scheme 5a.

Energy changes corresponding to Scheme 6 are shown in Fig. 1a. The energy of TS3-*o* is significantly large ($\Delta G^{\ddagger} = 55.25$ kcal/mol), and the route in Scheme 6 is obviously unfavorable energetically. Another route involving the different behavior of the two units $(PhO^-Na^+CO_2)_2$ needed to be investigated. Even in this new route, steps of precursor-*o* → TS1-*o* → Int1-*o* are included, because one CO_2 adduct is required for the reaction to progress.

Figure 2 shows one possible new path. Precursor-*o* consists of complexes $(PhO^-Na^+CO_2)_2$. The electrophilic addition of CO_2 to PhO^- occurs at TS1-*o*, which leads to Int1-*o*. In Int1-*o*, the proton H(8) in the trienone might be quenched by the phenoxide ion. Indeed, the proton movement was obtained as TS4-*o*. Subsequently, a disodium salicylate intermediate, Int4-*o*, was arrived at, which is quite similar to Int3-*o*; however, one point is crucially different

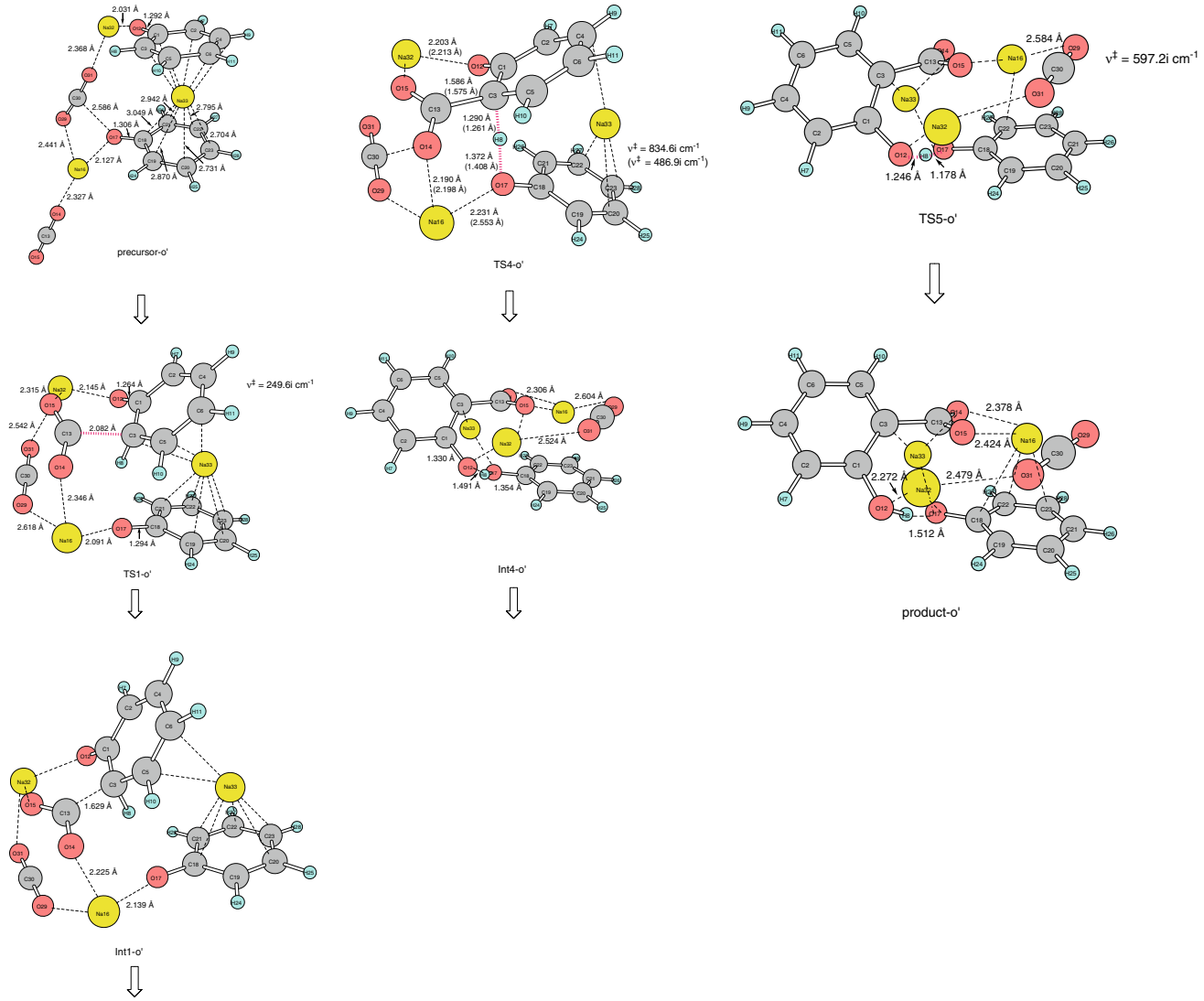

Fig. 4 Geometric changes in the $(PhO^{-}Na^{+}CO_2)_2 + Na^{+}$ model for the *ortho* channel

between Int3-*o* and Int4-*o*. In the latter, a strong hydrogen bond, O12—H8-O17, is formed. The formation is critical for the proton transfer, and in fact TS5-*o* was obtained. The product, sodium salicylate, was reached after TS5-*o*. Geometric changes along the route, precursor-*o* → Int1-*o* → Int4-*o* → product-*o*, in Fig. 2 are spontaneous and appear to be likely. Energy changes along the route in Fig. 2 are shown in Fig. 1b. The rate-determining step was found to be TS4-*o*, which is the deprotonation step of the trienone intermediate. The isomerization, Int4-*o* → product-*o* is very likely with the energy difference between Int4-*o* and product-*o* (=3.30 kcal/mol). If the difference was large, the unit (PhO^{-}, Na^{+} and CO_2) would undergo the second Kolbe–Schmitt reaction. The small energy difference indicates that the phenol may volatilize and go away (in Scheme 2) from Int4-*o* according to the Le Chatelier principle for the concentration in the equilibrium between Int4-*o* and product-*o*.

The calculated harmonic vibrational modes at approximately 1,600 cm^{-1} and their corresponding IR absorption intensities (Inten) of more than 100 KM/mole are given below.

For Int1-*o*,

ν (the 76th) = 1,633 cm^{-1} with Inten = 164,
ν (the 77th) = 1,642 cm^{-1} with Inten = 234,
ν (the 78th) = 1,668 cm^{-1} with Inten = 430,
ν (the 79th) = 1,695 cm^{-1} with Inten = 302.

For Int4-*o*,

ν (the 76th) = 1,589 cm^{-1} with Inten = 167,
ν (the 77th) = 1,629 cm^{-1} with Inten = 253.

For the former intermediate, ν (the 78th) has a remarkably large Inten(=430) and should have an intense peak in the IR spectra. On the other hand, for the latter, two peaks

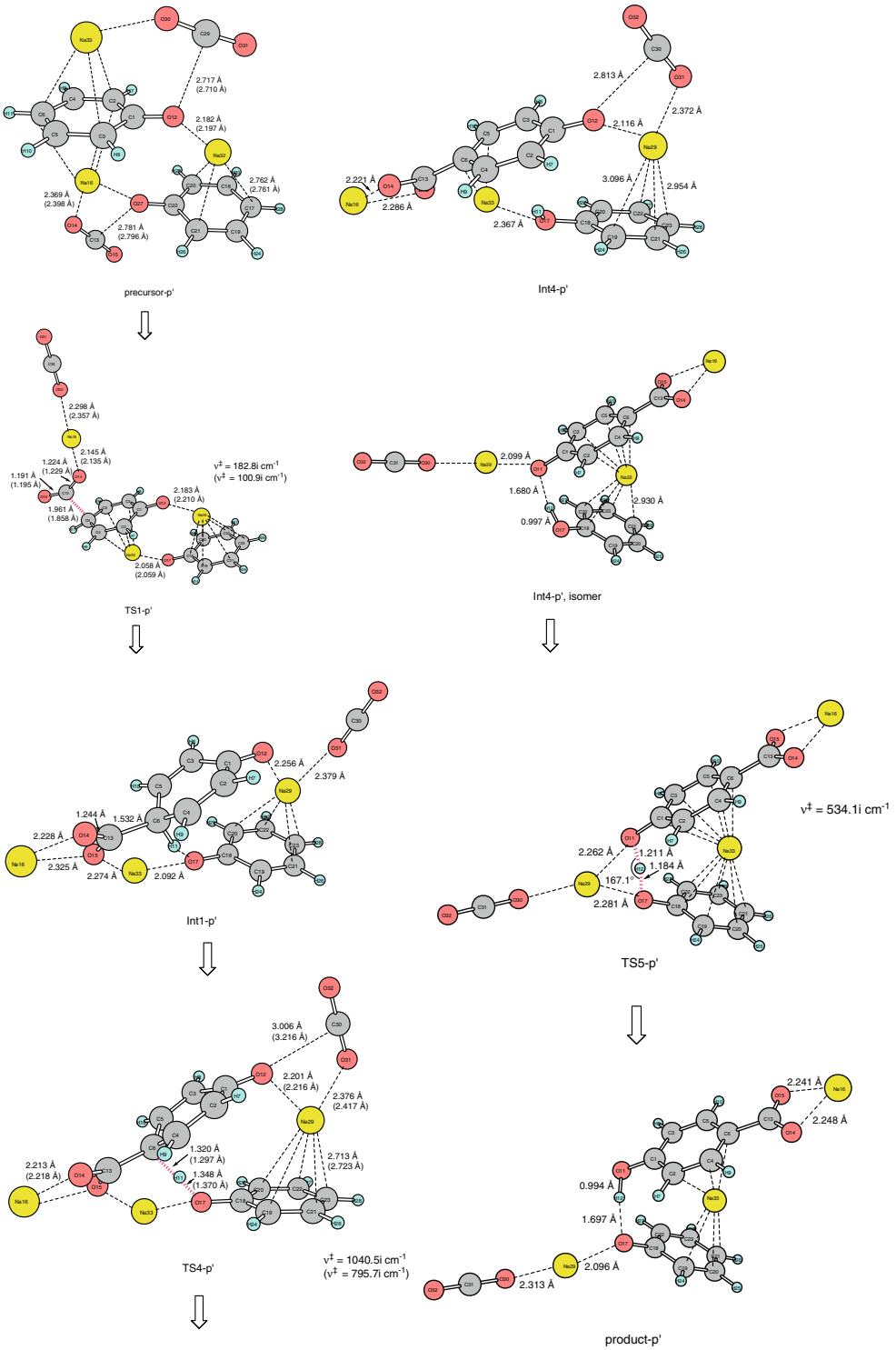

Fig. 5 Geometric changes in the $(PhO^{-}Na^{+}CO_2)_2 + Na^{+}$ model for the *para* channel

would be distinguishable, although the ν (the 76th) = 1,589 cm^{-1} is somewhat smaller than the experimental value [7].

The path to the *para*-hydroxybenzoic acid was sought, and geometric changes are shown in Fig. 3. Similar steps to those in Fig. 2, precursor-*p* → TS1-*p* → Int1-*p* → TS4-*p* → Int4-*p* → TS5-*p* → product-*p*, were obtained. Changes of Gibbs free energies are shown in Fig. 1. TS4-*p* has a significantly large energy, $\Delta G^{\ddagger} = 46.10$ kcal/mol. Also, product-*p* is remarkably unstable, $\Delta G^{\circ} = +24.45$

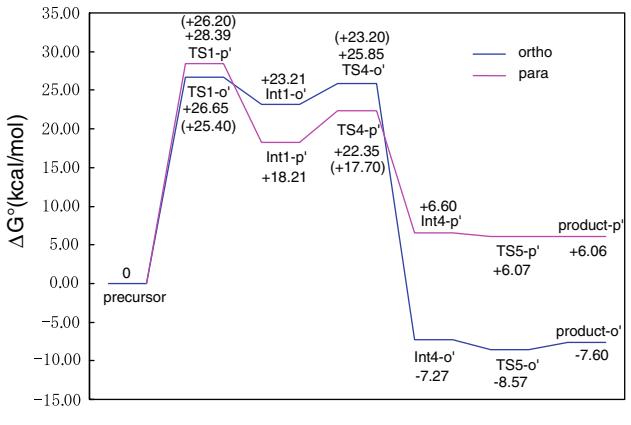

Fig. 6 Changes of Gibbs free energies of the $(PhO^{-}Na^{+}\text{-}CO_2)_2 + Na^{+}$ model. The corresponding geometries are shown in Fig. 4 (the *ortho* channel) and Fig. 5 (the *para* channel)

kcal/mol. The *para*-CO_2 addition route in Fig. 3 is, thus, improbable. The calculated result is inconsistent with the experimental one, the minor but detectable yield (4%) of the *para*-hydroxybenzoic acid [5].

3.2 Dimer model, $(PhO^{-}Na^{+}CO_2)_2$, catalyzed by a Na^{+} ion

In the previous sub-section, TS4-*o* and TS4-*p* (deprotonations from the CO_2 adducts) have been found to be rate-determining steps for *ortho* and *para* channels. Usually, the electrophilic addition is the rate-determining step (e.g., in benzene + NO_2^{+} → adduct → nitrobenzene + H^{+}). Along with the unreasonably large $\Delta G^{\ddagger}$ value of TS4-*p*, the dimer model alone seems not to describe properly the Kolbe–Schmitt reaction. At TS4, there are three anionic oxygens, which need to be stabilized by the counter ion Na^{+}. Then, three sodium ions are required for the stabilization (Scheme 7).

A $(PhO^{-}Na^{+}CO_2)_2 + Na^{+}$ model was adopted, and the *ortho* and *para* channels were investigated. Figs. 4 and 5 show geometric changes of the *ortho* and *para* channels, respectively. In the first geometry in Fig. 4 (precursor-*o*'), two sodium ions are bound to two PhO^{-} oxygen atoms and one ion is sandwiched by two PhO^{-} planes. Hereafter, the prime in e.g., precursor-*o*' shows the $(Na^{+})_3$ containing geometry. The *ortho*-channel process, precursor-*o*' → TS1-*o*' → Int1-*o*' → TS4-*o*' → Int4-*o*' → TS5-*o*' → product-*o*', is shown in Fig. 4. Similarly, the *para*-channel process, precursor-*p*' → TS1-*p*' → Int1-*p*' → TS4-*p*' → Int4-*p*' → TS5-*p*' → product-*p*', is shown in Fig. 5. In both channels, always at least one sodium ion is coordinated to the phenyl π cloud. The $\eta 6$ coordination seems to stabilize reacting systems.

Changes of Gibbs free energies in the $(PhO^{-}Na^{+}\text{-}CO_2)_2 + Na^{+}$ are shown in Fig. 6. First, energies of the *ortho* channel were compared to those in Fig. 1. $\Delta G^{\ddagger}$ (TS1-*o*') = +26.65 kcal/mol is similar to $\Delta G^{\ddagger}$(TS1-*o*) = +25.94 kcal/mol. On the other hand, $\Delta G^{\ddagger}$(TS4-*o*') = +25.85 kcal/mol is much smaller than $\Delta G^{\ddagger}$(TS4-*o*) = +35.67 kcal/mol. The third Na^{+} ion promotes the proton shift in TS4-*o* effectively. In addition, the third ion gives stabilization, $\Delta G°$(product-*o*') = −7.60 kcal/mol compared to $\Delta G°$(product-*o*) = +6.04 kcal/mol.

The effect of the third Na^{+} ion on the *para* channel is drastically larger than that on the *ortho* one. $\Delta G^{\ddagger}$ (TS1-*p*') = +28.39 kcal/mol is smaller than $\Delta G^{\ddagger}$

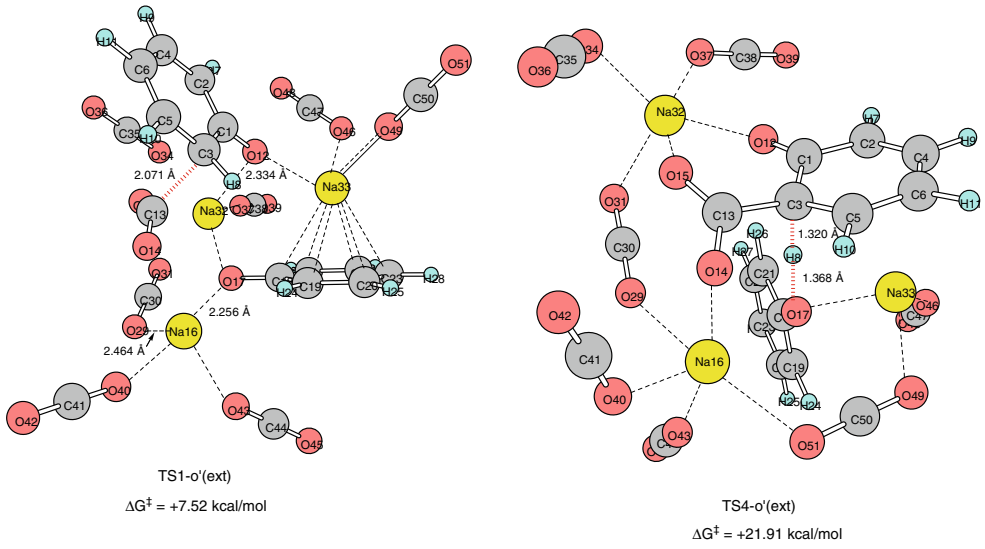

Fig. 7 Geometries and $\Delta G^{\ddagger}$ values of the CO_2 electrophilic addition TS, TS1-*o*'(ext), and the proton shift TS, TS4-*o*'(ext). The suffix, (ext), means the extended models of $[(PhO^{-}Na^{+}CO_2)_2 + Na^{+} + (CO_2)_6]$ of TS1-*o*' and TS4-*o*' in Fig. 4, respectively, which were calculated with RB3LYP/6-31G(d)

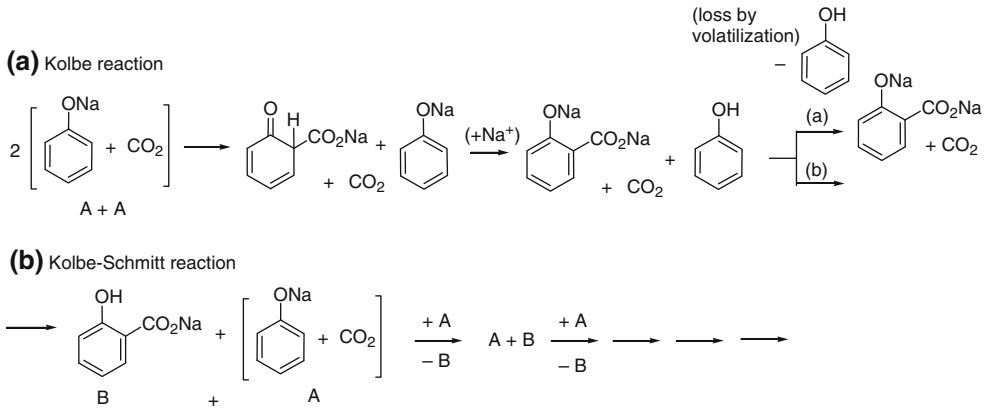

Scheme 8 Summary of the present computational study

(TS1-*p*) = +33.06 kcal/mol. More strikingly, $\Delta G^{\ddagger}$(TS4-*p*') = +22.35 kcal/mol is almost half of $\Delta G^{\ddagger}$(TS4-*p*) = +46.10 kcal/mol! $\Delta G°$(product-*p*') = +6.06 kcal/mol is much smaller than $\Delta G°$(product-*p*) = +24.45 kcal/mol. Therefore, when the third Na^+ ion is added to the $(PhO^-Na^+CO_2)_2$ systems, the para reactivity becomes close to the *ortho* one. Participation of the catalytic third ion to the dimer system has been found to enhance *ortho* and *para* products, which seems to be consistent with the result of the room temperature experiment [5]. While aggregation of counter ions is of low probability, its attainment gives a high reactivity of the Kolbe–Schmitt reaction.

In accordance with the CO_2 high pressure experiments [4, 5], a model composed of $(PhO^-Na^+CO_2)_2 + Na^+ + (CO_2)_6$ was considered. Since the system is large, B3LYP/6-31G(d) calculations were made on the three geometries corresponding to those of precursor-*o*', TS1-*o*' and TS4-*o*' of Fig. 4. The model calculation is needed, because the value of $\Delta G^{\ddagger}$ (TS1-*o*') = +26.65 kcal/mol is similar to that of $\Delta G^{\ddagger}$ (TS4-*o*') = +25.85 kcal/mol (Fig. 6) and the rate-determining step is unclear. Figure 7 shows results of the two TSs. $\Delta G^{\ddagger}$ (TS1-*o*'(ext)) = +7.52 kcal/mol is much smaller than $\Delta G^{\ddagger}$ (TS4-*o*'(ext)) = +21.91 kcal/mol. The CO_2 electronic addition was found to undergo the catalytic effect of the CO_2 solvation significantly.

4 Concluding remarks

In this study, the Kolbe–Schmitt reaction has been examined computationally. The Dewar's unimolecular model has been computed to be unlikely because of the significantly large activation energy for the [1, 3] hydrogen shift. A dimer model has been adopted. A path conserving the geometric symmetry has been assumed first. However, the path has a large energy for the proton shift (TS3-*o*), and one CO_2 adduct, i.e., trienone is decomposed to PhO^- and CO_2. Second, an unsymmetrical model has been investigated and a reasonable activation energy (=35.67 kcal/mol at TS4-*o*) has been obtained. A phenol intermediate is formed as a result of the proton acceptance from the trienone intermediate. The proton is shifted to the di-anion $^-OC_6H_4$-CO_2^- to form the product, sodium salicylate.

Addition of the Na^+ ion to the $(PhO^-Na^+CO_2)$ system gives rise to ready formation of sodium salicylate and sodium *para*-hydroxybenzoate.

The two units, $(CO_2 + Na^+ + C_6H_5O^-)$, have been computed to behave differently; one of them acts as a catalyst. The present reaction pattern, A + A → A + B shown in Scheme 8, seems to be a quite unique propagation.

References

1. Lindsey AS, Jeskey H (1957) Chem Rev 57:583
2. Kolbe H (1860) Ann Chem 113:125
3. Kolbe H (1874) J Prakt Chem Part 2 10:89
4. Schmitt R (1885) J Prakt Chem 31:397
5. Kosugi Y, Takahashi K, Imaoka Y (1999) J Chem Res (S) 114
6. Kosugi Y, Imaoka Y, Gotoh F, Rahim MA, Matsui Y, Sakanishi K (2003) Org Biomol Chem 1:817
7. Kunert H, Dinjus E, Nauck M, Sieler J (1997) Chem Ber/Recueil 130:1461
8. Hales JL, Jones JI, Lindsey AS (1954) J Chem Soc 3145
9. Dewar MJS (1949) The electronic theory of organic chemistry. Oxford University Press, London, pp 168–227
10. Markovic Z, Engelbrecht JP, Markovic S (2002) Z Naturforsch 57a:812
11. Marković Z, Marković S, Begović N (2006) J Chem Inf Model 46:1957
12. Marković Z, Marković S, Manojlović N, Predojević-Simović J (2007) J Chem Inf Model 47:1520
13. Marković Z, Marković S (2008) J Chem Inf Model 48:1–143
14. Woodward RB, Hoffmann R (1970) The conservation of orbital symmetry. Verlag Chemie, New York
15. Woodward RB, Hoffmann R (1965) J Am Chem Soc 87:395

16. Hirao I, Kito T (1973) Bull Chem Soc Jpn 46:3470
17. Yamabe S, Okumoto S, Hayashi T (1996) J Org Chem 61:6218
18. Becke AD (1993) J Chem Phys 98:5648
19. Lee C, Yang W, Parr RG (1988) Phys Rev B 37:785
20. Stephens PJ, Devlin FJ, Chabalowshi CF, Frish MJ (1994) J Phys Chem 98:11623
21. Perdew JP, Chevary JA, Vosko SH, Jackson KA, Pederson MR, Singh DJ, Fiolhais C (1992) Phys Rev B 46:6671
22. McLean AD, Chandler GS (1980) J Chem Phys 72:5639
23. Filatove M, Cremer D (2005) J Chem Phys 123:12410
24. Zhao Y, Schultz NE, Truhlar DG (2005) J Chem Phys 123:161103
25. Zhao Y, Truhlar DG (2008) Theor Chem Acc 120:215
26. Zhao Y, Truhlar DG (2008) Acc Chem Res 41:157
27. Zhao Y, Truhlar DG (2005) J. Chem Theor Comput 1:415
28. Woon DE, Dunning TH Jr (1993) J Chem Phys 98:1358
29. Kendall RA, Dunning TH Jr, Harrison RJ (1992) J Chem Phys 96:6796
30. Fukui K (1970) J Phys Chem 74:4161
31. Gonzalez C, Schlegel HB (1987) J Phys Chem 90:2154
32. Carpenter JE, Weinhold F (1988) J Mol Struct (THEOCHEM) 169:41
33. Gaussian 03, Revision C.02, Frisch MJ, Trucks GW, Schlegel HB, Scuseria GE, Robb MA, Cheeseman JR, Montgomery Jr. JA, Vreven T, Kudin KN, Burant JC, Millam, JM, Iyengar, SS, Tomasi J, Barone V, Mennucci B, Cossi M, Scalmani G, Rega N, Petersson GA, Nakatsuji H, Hada M, Ehara M, Toyota K, Fukuda R, Hasegawa J, Ishida M, Nakajima T, Honda Y, Kitao O, Nakai H, Klene M, Li X, Knox JE, Hratchian HP, Cross JB, Bakken V, Adamo C, Jaramillo J, Gomperts R, Stratmann RE, Yazyev O, Austin AJ, Cammi R, Pomelli C, Ochterski JW, Ayala PY, Morokuma K, Voth GA, Salvador P, Dannenberg JJ, Zakrzewski VG., Dapprich S, Daniels AD, Strain MC, Farkas O, Malick DK, Rabuck AD, Raghavachari K, Foresman JB, Ortiz JV, Cui Q, Baboul AG, Clifford S, Cioslowski J, Stefanov BB, Liu G, Liashenko A, Piskorz P, Komaromi I, Martin RL, Fox DJ, Keith T, Al-Laham MA, Peng CY, Nanayakkara A, Challacombe M, Gill PMW, Johnson B, Chen W, Wong MW, Gonzalez C, Pople JA (2004) Gaussian, Inc. Wallingford CT
34. Stanescu I, Achenie LEK (2006) Chem Eng Sci 61:6199